The velocity dispersion amongst the nebulae in the LMC is not significantly different from the velocity dispersion within the 30 Doradus nebula, $11 \cdot 3 \pm 3 \cdot 2$ (s.e.) km/sec (Feast 1961).

The low-velocity dispersion found for young objects in the LMC implies that if the axis of rotation makes only a small angle with the line of sight, as is the case in de Vaucouleurs' model, then the system of nebulae and supergiants must be highly flattened to the plane.

Further work on emission nebulae in the Clouds is in progress. Some low dispersion spectra of faint nebulae far out along the major axis of the LMC have been obtained and it is also intended to use the coudé plates to derive relative intensities of the [OII] ultraviolet lines and to deduce electron densities from these measurements.

References

FEAST, M. W. (1961).—*M.N.* **122**: 1–16.
FEAST, M. W., THACKERAY, A. D., and WESSELINK, A. J. (1960).—*M.N.* **121**: 337–85.
FEAST, M. W., THACKERAY, A. D., and WESSELINK, A. J. (1961).—*M.N.* **122**: 433–53.

Discussion

Woolley: Have you considered the effect on the curve of rotation of a change in Θ_c?

Feast: I have used the same figure 270 km/sec as in our previous paper in order to obtain a quick comparison. When we wrote the previous paper, we considered the question and decided that any reasonable variation of the value should not affect the rotation curve.

Aller: Which nebular spectral lines did you use?

Feast: Mostly the [OII] lines. These are the strongest lines in the photographic region. We sometimes measured the Balmer lines or [NeIII] for the brighter nebulae.

Aller: Did you find any evidence for internal motions (doubling or deformation of lines) or different velocities for the green nebular lines of [OIII] and [OII] λ3726, 3729?

Feast: I did not measure the green nebular lines on the coudé. I do not think we can say anything about differential motion from the present measurements. There is, of course, a conspicuous variation in electron density.

Kerr: I would like to summarize the present position regarding radio evidence on the kinematics of the Clouds. The rotation curve for the Large Cloud derived from the 1960 observations agrees fairly well with the 1953 results, but the analysis of the later observations was not pushed very far, because high-resolution studies were just beginning. Optical and radio rotation velocities can now be compared more systematically by isolating smaller areas.

Buscombe: There is tantalizing though slender evidence that the SMC globular clusters share a distribution of higher velocities than the supergiants, relative to the Sun.

57. COMPARISON OF STELLAR ORBITS IN THE LARGE MAGELLANIC CLOUD AND IN THE GALAXY

L. PEREK
Astronomical Institute of the Czechoslovak Academy of Sciences

The rotation curves of the LMC and the Galaxy differ markedly by the slope of the curve near the centre. Two causes may be responsible for this difference. Firstly, the mass of the Galaxy exceeds that of LMC by about one order of magnitude

and the resulting orbital velocities at corresponding distances must be larger in the Galaxy than in the LMC. Secondly, the distribution of mass may be different in the two systems. Indeed, several investigations showed that the Galaxy is best represented by a model exhibiting a strong concentration of mass while the LMC is consistent with models of a very weak concentration, a homogeneous spheroid yielding a passable approximation.

Fields of gravity of stellar systems are rather complicated and are known with a relatively low accuracy. Especially in the case of the Galaxy the presence of several populations with substantially differing space distributions makes it impossible to express by a simple mathematical formula the field of gravity in a region sufficiently large for investigating stellar orbits. It seems to be a question of a short time before different populations will have to be respected in studies of the dynamics of Magellanic Clouds and a similar situation will arise there also.

Models of stellar systems consist generally of several superposed geometrical bodies ranging from mass points to heterogeneous spheroids. Solutions for stellar orbits in such elaborate models are generally beyond the scope of analytical methods and can be attempted only by numerical computations. The advantage of electronic computers in dealing with fields of any form is, on the other hand, paid for by the loss of generality. It seems that analytical investigations of stellar orbits in simple fields of gravity, roughly approximating those of stellar systems, have been neglected although relations can be derived between general properties of the orbits and main features of the assumed distribution of mass.

Two relatively simple models were investigated recently (Perek 1962*a*,*b*), one approximating the field of gravity of the LMC, the other applied with success to the Galaxy.

Both models are heterogeneous spheroids with finite masses and dimensions. Equations of motion were solved in terms of elliptic functions for mass points moving in the plane of symmetry and inside the model.

In the first case the density is of the parabolic form

$$\rho = \rho_c \ (1 - m^2),$$

where ρ_c is the density at the centre and the parameter m specifies a spheroidal shell similar to the basic spheroid of semi-axes a, c, i.e.

$$m^2 = \frac{R^2}{a^2} + \frac{z^2}{c^2},$$

R and z being cylindrical coordinates.

The second, hyperbolic case, is given by

$$\rho = \rho_0 \left(\frac{1}{m} - 1 \right),$$

where ρ_0 is the density at $m = \frac{1}{2}$. The two density laws are shown in Figure 1. Both models are limited by their physical border, i.e. by the spheroid of zero density, $m = 1$. This is the reason why all results apply only to internal points. The models differ by the degree of concentration of the mass. In the first case the density decreases with the distance from the centre very slowly along a parabola. Kerr and de Vaucouleurs (1955) and later Feast, Thackeray, and Wesselink (1961) found

a good fit of a model of this kind with the rotation curve observed in the LMC with a semi-axis $a=3.^{\circ}5$. In the second case the density law is represented by a hyperbola with an infinite density at the centre decreasing rapidly with the distance. A composite model of four spheroids of this kind was applied by Schmidt (1956) to the Galaxy.

Table 1 gives the comparison of principal formulae valid for the two models with those of the two-body problem. The constants α and β contain the constant of gravity, the mass of the model, and the axial ratio c/a. The potential was defined so as to make the attraction positive.

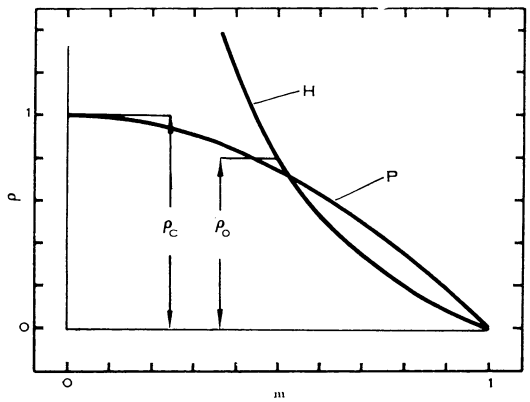

Fig. 1.—The parabolic (P) and hyperbolic (H) density laws. The two models shown have the same total mass.

The equation of motion is solved in the two-body problem by means of a well-known substitution leading to circular functions. In the case of the spheroids, there appear polynomials of a degree higher than 2 under the root-sign and elliptic functions must be resorted to. The constant k depends on the initial velocity and h is the constant of areas.

The solution in the two-body problem is a conic section. An explicit form of the true anomaly was used here, in analogy to the spheroidal cases. In the parabolic case Weierstrassian p-function is introduced by the substitution where v is a constant. The relation between the new independent variable w and time t is particularly simple. An equality sign cannot, however, be put between the two variables. For orbits contained inside the spheroid they differ by an imaginary constant. In the hyperbolic case the substitution is a linear rational function in terms of the p-function where u_1, u_2 are constants depending on initial conditions.

A mass point cannot be superposed on the spheroid with parabolic density law because a linear term would appear under the root sign in the equation of motion, thus making the substitution ineffective. On the other hand, in the hyperbolic spheroid a superposition of a mass point does not change the degree of the polynomial and only the invariants of the p-function and the constants u_1, u_2 are changed.

TABLE 1

PRINCIPAL FORMULAE

Model	Mass Point	$\rho=\rho_c\,(1-m^2)$	$\rho=\rho_0\,(\frac{1}{m}-1)$
Potential	$-\frac{\alpha}{R}$	$-\frac{1}{2}(\gamma-\alpha R^2+\beta R^4)$	$-\frac{1}{2}(\gamma-\alpha R+\beta R^2)$
Attraction	$\frac{\alpha}{R^2}$	$\alpha R-2\beta R^3$	$\frac{1}{2}\alpha-\beta R$
Circular velocity	$\sqrt{\frac{\alpha}{R}}$	$R\sqrt{\alpha-2\beta R^2}$	$\sqrt{R\,(\frac{1}{2}\alpha-\beta R)}$
Equation of the orbit	$\pm\mathrm{d}\theta=\frac{h\mathrm{d}R}{R\sqrt{kR^2-2\alpha R-h^2}}$	$\pm\mathrm{d}\theta=\frac{h\mathrm{d}R}{R\sqrt{\beta R^6-\alpha R^4+kR^2-h^2}}$	$\pm\mathrm{d}\theta=\frac{h\mathrm{d}R}{R\sqrt{\beta R^4-\alpha R^3+kR^2-h^2}}$
Substitution	$R=\frac{a(1-e^2)}{1+ew}$	$R^2=\frac{1}{\beta}(pw-pv)$	$R=R_0\,\frac{pw-pu_1}{pw-pu_2}$
Transformed equation of the orbit	$\pm\mathrm{d}\theta=\frac{\mathrm{d}w}{\sqrt{1-w^2}}$	$\pm\mathrm{d}\theta=h\beta\frac{\mathrm{d}w}{pw-pv}$ $\mathrm{d}t=\mathrm{d}w$	$\pm\mathrm{d}\theta=2\frac{h}{R_0}\frac{pw-pu_2}{pw-pu_1}\mathrm{d}w$ $\pm\mathrm{d}t=2R_0\frac{pw-pu_1}{pw-pu_2}\mathrm{d}w$
Solution	$\pm\theta=\cos^{-1}(\frac{p}{ew}-\frac{1}{e})$	$\pm\theta=\frac{i}{2}\log\frac{\sigma(w-v)}{\sigma(w+v)}+iw\zeta v$ $t=w+\text{imag. const.}$	$\pm\theta=i\log\frac{\sigma(w-u_1)}{\sigma(w+u_1)}+2w(\frac{h}{R_0}+i\zeta u_1)$ $+t=\frac{1}{\sqrt{\beta}}\log\frac{\sigma(w+u_2)}{\sigma(w-u_2)}+2w(R_0-\frac{1}{\sqrt{\beta}}\zeta u_2)$

It is even possible to suppress the original spheroid and check the reduction of the orbits to Keplerian ellipses.

Because of the periodicity of elliptic functions,

$$p(w+2\omega_1)=pw,$$

where $2\omega_1$ is the real period, the two above arguments lead to identical distances R. Thus the real period is related to the anomalistic period of the orbit. The solution yields the true anomaly ϑ and time t as functions of w expressed in terms of Weierstrassian functions σ and ζ. These functions are defined by quadratures of the p-function. The increase of ϑ corresponding to $2\omega_1$ defines the relative position of the subsequent loops of the orbit; thus the rotation of the line of apsides can be followed.

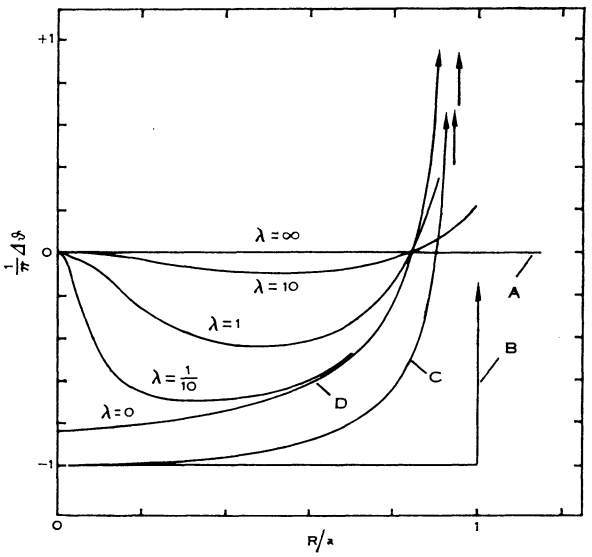

Fig. 2.—Rotation of the line of apsides for a mass point (A), for a homogeneous spheroid (B), for a heterogeneous spheroid with parabolic (C), and hyperbolic (D) density distributions.

For circular orbits the Weierstrassian functions degenerate to circular or hyperbolic functions but the real period retains its significance and so does the rotation of the line of apsides. Its value can be easily computed for circular orbits and it is the limit of apsidal rotation of nearly circular orbits.

In an analogy with Keplerian orbits the definition was adopted that there is no apsidal rotation if the subsequent extreme distances lie 360° apart. This is shown by the straight line A in Figure 2 which is valid for the two-body problem. A homogeneous spheroid has orbits in the form of central ellipses, the extremes following after half a revolution, i.e. 180°. If the spheroid is sufficiently flattened a zone of unstable circular orbits begins at the boundary of the spheroid. This is shown by line B. The spheroid with parabolic density is well approximated by the homogeneous

spheroid near the centre and the apsidal rotation starts at $-180°$. However, the distance between subsequent loops begins to decrease with increasing distance and the curve C eventually crosses the zero line. At that point the orbits are similar to Keplerian ellipses in having the extremes always at the same position angle. The curve increases further; the number of revolutions necessary for the completion of one anomalistic period grows until it becomes infinite at the beginning of the zone of unstable circular orbits. An unstable circular orbit starts from the asymptotic circle by an unwinding spiral, it makes a loop around the centre, and it returns on a mirrored spiral back to the asymptotic circle. Although the entire orbit affords infinite time, the stars spend only the time of a few revolutions at a marked distance from their asymptotic circles.

The orbits inside a spheroid with hyperbolic density law cannot be approximated by central ellipses anywhere. Right from the smallest orbits they possess a definite amount of apsidal rotation different from $-\pi$ (curve D, $\lambda=0$). Otherwise they behave qualitatively in analogy with the preceding case.

If a mass point is superposed on this spheroid, the curve is changed essentially. Denoting λ the ratio of the mass point to the mass of the spheroid, the figure shows that even a small central mass changes small orbits completely. Its influence is felt even at the border because it makes the zone of unstable circular orbits thinner or eliminates it altogether. However, the central mass does not shift the point of zero apsidal rotation.

The main difference between systems with a low and a high degree of concentration of mass is in the mixing of stars. Mixing in position angle is complicated and a more detailed analysis would be needed. On first sight it appears that any commensurability in the apsidal rotation reduces the degree of mixing. Thus the degree of mixing will be different at different zones according to the distribution of mass.

Radial mixing is dependent on the degree of approach to the centre. Let us compare orbits starting at apocentre with half the circular velocity. For a Keplerian ellipse the ratio of distances at pericentre and apocentre is $R_p/R_a=0\cdot14$. For the parabolic density law this value ranges between $0\cdot33$ and $0\cdot50$ according to the size of the orbit. Respective figures for the hyperbolic density law are $0\cdot26$ and $0\cdot43$. The range of velocities permitting the passage of a star through the central bulge is in actual systems much more restricted than in the two-body problem.

Thus in comparing the two stellar systems we should expect less mixing in the LMC than in the Galaxy. Especially in the radial mixing the present analysis shows a definite difference between the two assumed density distributions.

References

FEAST, M. W., THACKERAY, A. D., and WESSELINK, A. J. (1961).—*M.N.* **122**: 433–53.
KERR, F. J., and DE VAUCOULEURS, G. (1955).—*Aust. J. Phys.* **8**: 508–22.
PEREK, L. (1962*a*).—"Vistas in Astronomy." (Ed. A. Beer.) Vol. 5. pp. 28–39. (Pergamon Press: Oxford.)
PEREK, L. (1962*b*).—*B.A.C.* **13**: 211–17.
SCHMIDT, M. (1956).—*B.A.N.* **13**: 15–41.

Discussion

Lindblad: I have seen your results with great interest. It is interesting to note that they apply also to the Large Magellanic Cloud. Though this is a schematical presentation it can give a general orientation to the problem.

Perek: The purpose of this work was to obtain the relation between the general properties of orbits and the general features of various mass distributions. I have not attempted to obtain numerical values.

58. COMPARISON OF THE MAGELLANIC CLOUDS WITH OTHER IRREGULAR BARRED SPIRALS

G. DE VAUCOULEURS
University of Texas

I. The main structural characteristics of the irregular barred spirals of the magellanic type are illustrated in Figure 1. They were first detected 10 years ago on small-scale photographs of the Large Cloud taken at Mount Stromlo (de Vaucouleurs 1954, 1955) and were later found to be uniformly present in many other "late-type" barred spirals designated SB(s)d and SB(s)m in the revised classification system (de Vaucouleurs 1959). These stages form a continuous transition between the regular barred spirals of the "S-shaped" sequences, such as NGC 1365: SB(s)b, NGC 1300: SB(s)bc, NGC 7479: SB(s)c, and the completely irregular system IBm showing only an axial bar and little or no traces of whorls, such as NGC 4449 and 4214. Examples of the transition stages are NGC 7741: SB(s)cd, NGC 1313: SB(s)d, NGC 4027: SB(s)dm, NGC 4618: SB(rs)m, and the Large Magellanic Cloud: SB(s)m (Fig. 2). The Small Cloud, because of its interaction with the Large Cloud and its

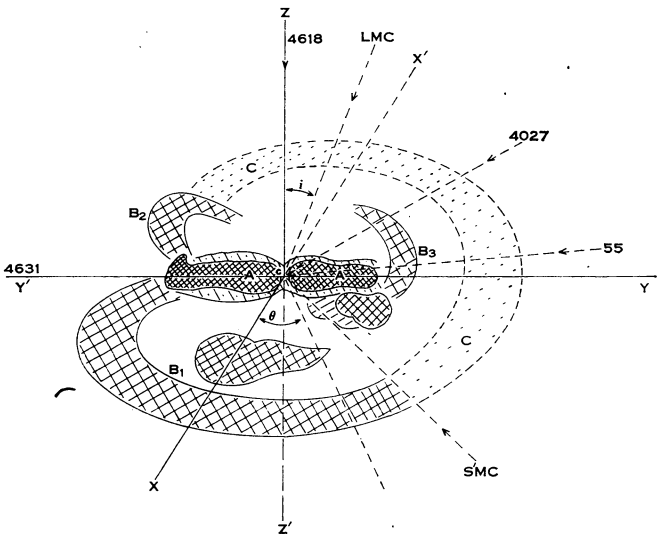

Fig. 1.—Structure of SB(s)m galaxies, and coordinate system.

https://doi.org/10.1017/S0074180900052694 Published online by Cambridge University Press